1. Aims and purposes of the satellite

Marine debris, especially microplastic has a fatal effect on ecology. In recent years, million metric tons of plastic waste was dumped into the ocean, the most harmful one is the plastic particles among 0.5 mm to 5 mm, call “microplastics”. Microplastic can be divided into first and secondary classes by the way they were generated. First-class microplastic was manufactured in the form of particles, and secondary class microplastics were generated through the degradation of larger plastic debris. In addition to its own toxicity, microplastics have a larger area to volume ratio than macroplastics and are more susceptible to contamination by environmental pollutants. Since microplastics are made of highly hydrophobic materials, the chemical pollutants are concentrated on their surfaces, and microplastics act as reservoirs of toxic chemicals. By eating the contaminated microplastics, individuals are susceptible to physical damage. Marine organisms at every level of the marine food web ingest microplastics. After humans, which is on the top of the food chain, catch those marine organisms and consumed, the microplastics and chemical toxicity will finally cause damage to our health. There is still not an effective solution to resolve this problem. The first step to resolve this problem is to investigate the information about marine debris, including position, component, size, and density. International scientific community launched an activity in 2019, called Integrated Marine Debris Observation System (IMDOS). The target of the mission is to monitor the distribution of ocean debris and evaluate the jeopardize to the environment and compensated for the error of marine debris numerical models by acquiring the concentration, component, size, and source information of marine debris. The mission takes satellites, airplanes, UAVs, buoys, benthic landers, and shoreline monitoring as observing planform. A journal about this activity had published in August 2019[1]. It pointed out there were some on-orbit satellites had been used to observe marine debris, but the result was not as expected. The main reason was that the satellites did not meet the requirement for ocean debris observation, which including spectral resolution, spectral range, sensitivity, revisit time, geospatial resolution, and converge. Recently, marine debris remote sensing satellite is still in the startup stage and there is no space institution having any mission about this in the short term. Our mission- Global Ocean Microplastics Intelligence remote-sensing SATellite is to compensate for such shortage.

The main mission objective of the Global Ocean Microplastics Intelligence remote-sensing SATellite (GOMI SAT) is to observe global surface microplastics. Using short wave infrared (SWIR) spectral camera in combination with data (ocean surface temperature, wave height) of Global Navigation Satellite System-Reflectometry (GNSS-R) to investigate the relation between microplastics and ocean current, searching the spatial distribution characteristics and temporal characteristics of microplastics. Moreover, GOMI SAT takes advantage of the AI recognition system to reduce the data volume effectively. In the past decades, scientists and engineers tried to collect large area marine debris data using remote sensing on aircraft or take samples by towing techniques. However, in comparison with the whole ocean coverage, the coverage of missions performed before was too small, and the samples were only taken on specific time thus didn’t have dynamic characteristics of marine debris, the position change due to ocean current was ignored. Although the numerical model can greatly improve the weak coverage and temporal distribution of the survey, it

did not have good enough accuracy. In current marine debris numerical models, ocean circulation, atmospheric circulation, global warming effect even human activity has to be taken into account, the extremely complex interaction between marine and environment makes numerical models are difficult to visualize the global scales distribution with high accuracy. And this problem is also one of the GOMI SAT's goal, to provide enough data to modify the current numerical models.

One of the main difficulties currently as a challenge of understanding the marine debris is the poor coverage of the existing studies. Its poor coverage makes mostly study and observation be hard to conduct. Most of the information about the spatial distribution of marine debris comes from numerical models. According to the latest spatial distribution result of marine debris sampling, the resource is from table 1, on North Pacific Gyre, the coverage of marine debris is 0.02% to 0.00002%. Although the lack of data, the emergence of marine debris can be predicted. According to the two approaches of NASA's experiment results, the first data comes from the floating scientific buoys that NOAA has been distributing in the oceans for the last 35-year, the second one is the computational model of ocean currents called ECCO-2, releasing particles evenly around the world and let the modeled currents drive the particles. The results in figure 1 and figure 2 show that there are five garbage patches (accumulation zones): Indian Ocean Garbage Patch, North Atlantic Garbage Patch, North Pacific Garbage Patch, South Atlantic Garbage Patch, South Pacific Garbage Patch. Apparently, the accumulation zones have a close connection with ocean currents. Most marine debris numerical models consider the ocean currents as an input parameter, which has an enormous impact on the simulation results. The accuracy of the ocean current parameter thus acts as a key error source. GOMI SAT has a GNSS-R to obtain the information such as wind speed on the sea surface and wave height of ocean currents as observing marine debris. These data can provide better accuracy for numerical models. Moreover, the interaction mechanism between ocean currents and marine debris can be explored deeply.

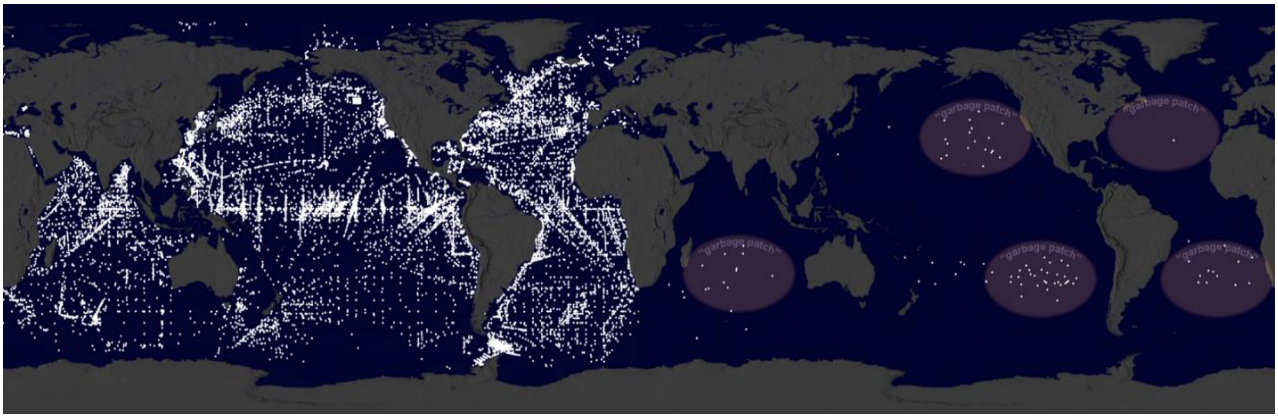

Figure 1 Scientific buoys that NOAA has been distributing in the oceans for the last 35-years represented here as white dots. The left part of the figure shows the position of buoys at the start time. The right part of the figure presents the position after 2000.[3]

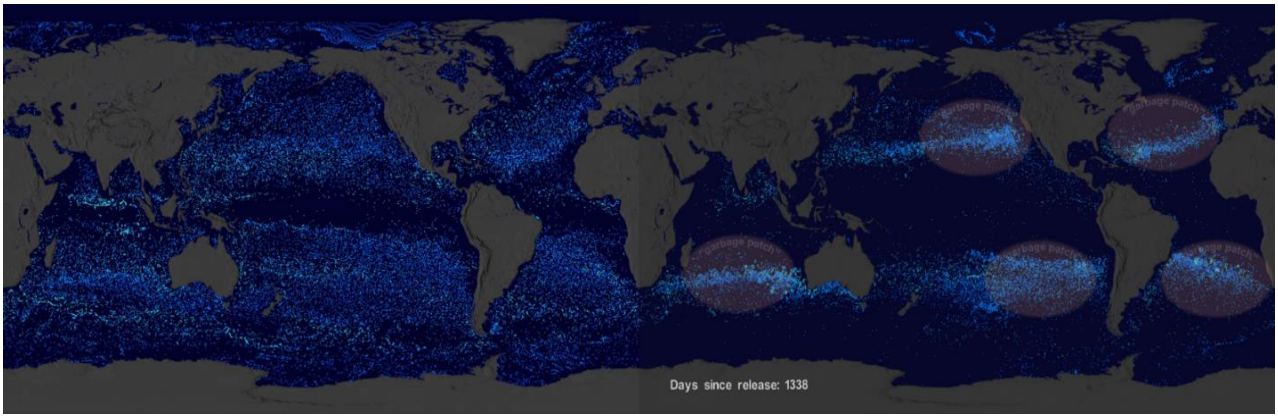

Figure 2 Simulation of surface marine debris using a computational model of ocean currents called ECCO-2. Releasing particles evenly around the world and let the modeled currents carry the particles. Although the duration of buoys and particles in the simulation are not the same, the results show that ocean circulation has a huge impact on surface marine debris.[3]

On temporal distribution characteristics, there is not much information about the marine debris on their temporal variations and spatial distributions, most of its available information is currently based on numerical models. Rivers and continental watershed have been proven that have seasonal variations. When the rainy seasons come, a large amount of rain drags the debris accumulates into the riverine during dry seasons into the ocean. However, for open ocean areas, the temporal variation is still unclear. In garbage patch, seasonal change of the concentration of marine debris also lacks related information and exploration. Now that there is proof of rivers, which is the input of marine debris, has seasonal variations, if the information with a high temporal resolution can be carefully investigated, it can greatly help to understand the transportation mechanism of marine debris. The information about variations of coverage in accumulation zones is also sparse. Coverage of marine debris in open ocean areas changes with several factors such as biofouling or vertical mixing effect. GOMI SAT cannot get the information of marine debris under the sea surface, but observing coverage variations with time will help to understand the vertical motion of marine debris to a certain extent. In the long term, there are some phenomena that have significant impacts on ocean currents. For example, El Niño-Southern Oscillation (ENSO) and Quasi-Decadal Oscillation (QDO). If these phenomena are taken into consideration, the periods of that are about 3~5 years and 8~12 years respectively, To investigate more deeper about interaction between ocean temperature and plastic marine debris, 5 years mission is desired. If the satellite can operate about 10 years, we can get more information.[2]

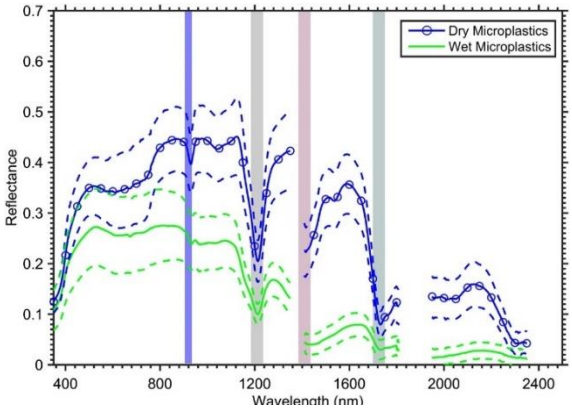

Figure 3 An airborne remote sensing case study of synthetic hydrocarbon detection using short wave infrared absorption features identified from marine-harvested macro- and microplastics. P.229

Marine debris covers a wide range of sizes, composition as well as density, and the complex characteristics make research complicated. However, according to the results of RESMALI (Remote Sensing for Marine Debris) [2], “plastic” marine debris is the main component of marine debris, especially in the ocean surface waters (> 90%). Due

to this reason, investigation on the plastic marine debris is our main objective and microplastic is the most representative of plastic marine debris. By the observational data from RESMALI, maximums of marine debris concentrations are found for the range between 0.5mm to 5mm, which is microplastics, which also the most harmful one among marine debris. After plastic marine debris entering the ocean, it suffers from mechanical degradation and UV radiation degradation thus breakdowns into smaller pieces. Since the microplastics are caused by degradation, it hardly can generate buoyance by its own shape to float on the ocean surface. The microplastics floating on the ocean surface is mostly made of Polypropylene (PP) and Polyethylene (PE), which have a density lower than seawater. The size of microplastics is mainly between 0.5mm-5mm, it is obviously impractical to identify microplastics by using high-resolution images. Therefore, the payload must be designed specifically to fit the optical properties of microplastics. At present, the reflection spectrum research on PP and PE plastics is more detailed than other optical properties, so the reflection spectrum of microplastics was focused on the design of the payload. According to research, PP and PE plastics have several absorption lines at the SWIR frequency (Figure 3), and seawater has low reflectiveness at SWIR. Therefore, the main payload would be two SWIR camera. One observes absorption lines, and another observes reflection lines. However, there is another challenge: the coverage area of microplastic on the ocean surface is extremely low. According to the practical sampling report, the coverage ratio varies from 0.02% to 0.00002% (Table1). To successfully detect microplastic, there are two approaches, one is to shoot at a higher resolution so that the aggregated microplastics can reach a sufficient coverage for the camera detection, and the other one is to use a larger pixel size, improve the signal-to-noise ratio (SNR) of the camera. Since our mission goal is to observe the microplastic distribution in a wide area of the world, the large amount of data transmission caused by high resolution images is not practical for the size of our satellite, and the large mirror required for a high resolution is also difficult in the design for the satellites of this size. At the same time, the horizontal resolution required by the marine debris motion model is not high. In summary, the main payload of our observation of microplastic equips two high-SNR low-resolution cameras those observe at the wavelength of the absorption and reflection lines of the microplastics in the SWIR band. In addition, the distribution and movement patterns of microplastic are strongly associated with ocean currents, waves, wind fields, and seawater density. Therefore, a GNSS reflectometry is placed to observe the wave height of the ocean, wind speed on the sea surface, and a thermal camera to observe the temperature of the ocean surface is also programmed. Because the signal of microplastic is extremely weak, the influence of clouds is critical in this mission. To reduce the disturbance of clouds on observations, a CMOS visible-light camera would cooperate with the thermal camera to detect clouds.

Table 1. RESMALI Remote Sensing for Marine Litter. P25

Region	Size interval (cm)					Source	Macrodebris sampling
	0-2 cm	2-10 cm	10-30 cm	> 30 cm	Total		
North Pacifc (low range)	0.00000%	0.00000%	0.00000%	0.00002%	0.00002%	Goldstein et al. 2012	Visual census
Near-shore Med waters	0.00012%	0.00021%	0.00026%	0.00021%	0.00080%	MIDAS project (unpublished)	Mega-net
North Pacifc (high range)	0.00040%	0.00100%	0.00320%	0.01540%	0.02000%	Goldstein et al. 2012	Visual census

In summary, the stagnation of marine debris research causes by the poor spatial and concentration distribution information and temporal resolution data, in addition to the large

uncertainty in numerical models. The GOMI SAT mission is proposed to have a comprehensive investigation on marine debris characteristics above and is expected to achieve the following goals:

(1) To detect the position of plastics marine debris.
(2) To measure the concentration of plastic marine debris which larger than 0.01% coverage.
(3) To acquire high temporal resolution data with one-day revisit time.
(4) To measure wave height, the temperature of ocean currents, and local wind speed which are highly related to the motion of plastic marine debris.
(5) To construct a global plastic marine debris distribution and to provide accurate observation data to improve numerical models.
(6) A 5+5 years lifetime of GOMI SAT constellation is expected.

2. Design Result

2.1. Orbital Analysis

To achieve the goal of global ocean coverage and a high temporal resolution, the GOMI SAT mission is programmed as a constellation of six 6U CubeSats. The type of the constellation orbits is selected as sun-synchronous, six CubeSats are at the same altitude with 725 km height, the argument of periapsis between each CubeSat is 60 degrees as figure 4 presents. The orbital parameters of GOMI SAT constellation are listed in table 2.

Table 2. Orbit Elements of the GOMI SAT Constellation of 6 CubeSats

Orbit Type	Sun-synchronous
Altitude (km)	725
Argument of Periapsis (deg)	0, 60, 120, 180, 240, 300
Orbit Period (s)	5957.803

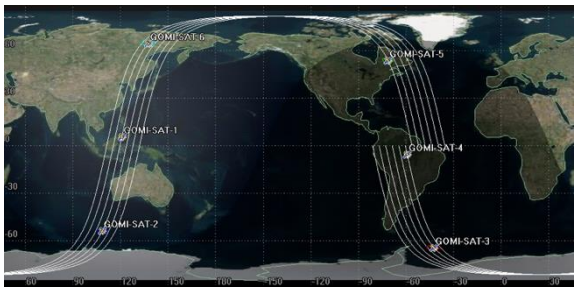

Figure 4 The orbit trajectories of the constellation

2.2. Coverage Analysis

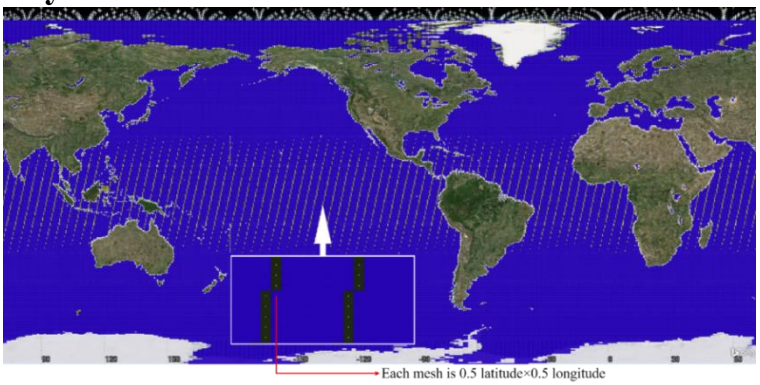

Figure 5 Result of coverage analysis, blue color marks the surveyed area, and it shows that the requirement of the one day revisit time is achieved.

To demonstrate the feasibility of this mission, Coverage Figure of Merit Object, a tool for modeling the coverage of remote-sensing satellite under STK is used to perform the coverage analysis of the GOMI SAT mission. The global ocean including lake within the continent is set as the coverage analysis target first. To get higher accuracy, the point granularity of coverage is set to

0.5 latitude×0.5 longitudes. For the SWIR camera onboard satellites, the sensor is a rectangle shape and the field of view angle is set to 29°×22°. The detailed design of the SWIR camera will be presented clearly in the later section. Since the SWIR camera must detect the reflectance signal of plastic marine debris and ocean surface, it cannot operate at umbra and penumbra interval and the camera must be turned off in these intervals. The revisit time is programmed as two days in the early design. However, after the simulation shown in figure 5, it is confirmed that the global survey can be done in one day if a carefully programmed attitude control is taken into account. The approach of attitude control to achieve this goal is also discussed in the later section. In summary, after analyzing the mission orbits and ground coverage, our GOMI SAT constellation can indeed complete a global ocean survey with a revisit time of 1 day and satisfy the requirement of the mission.

2.3. The GOMI SAT system

The GOMI SAT mission consists of three units including space, ground, and launch segments. The space segment is the six identical 6U-CubeSats with 6 subsystems and 4 sensors as its payloads. The ground segment includes an S-band ground station operated by the National Space Organization, Taiwan, as well as a UHF ground station, a Mission Control Center (MCC), and a data distribution center operated by the National Cheng Kung University. The launch segment is the JAXA H-IIA and the GOMI SAT microsats are expected to be launched in a piggy-back form.

There are 6 subsystems in GOMI SAT CubeSats, including **S**tructure and **M**echanisms **S**ubsystem (SMS), **T**hermal **C**ontrol **S**ubsystem (TCS), **A**ttitude **D**etermination and **C**ontrol **S**ubsystem (ADCS), **E**lectrical and **P**ower **S**ubsystem (EPS), **T**elemetry and **T**racking and **C**ommand subsystem (TT&C), and **C**ommand and **D**ata **H**andling subsystem (C&DH). Four scientific sensors are placed onboard the GOMI SAT CubeSats, including a SWIR (Short-Wave Infrared) camera, a CMOS (Complementary Metal-Oxide-Semiconductor) camera, a thermal camera, and a GNSS-R (Global Navigation Satellite System Reflectometer). Details of the sensors are discussed in the later session.

Table 3. Mass budget, the mass of each component and the total mass of GOMI SAT CubeSat.

Component	Qtn	Unit Weight (g)	Component	Qtn	Unit Weight (g)
Skeleton	1	1100	iPDU	1	57
Panels	10	80	S-band transmitter	1	132
Pipe & strap	1	700	S-band antenna	1	50
Radiator	1	110	UHF receiver	1	25
XACT50	1	1394	UHF antenna	1	30
MEPSI	1	456	SWIR cam	2	528
iOBC	1	94	CMOS cam	1	85
Protector	1	110	Thermal cam	1	27
Solar Cell	128	4	GNSS-R	1	80
iPCU	1	58	GNSS-R antenna	4	40
iPBU	1	49	Harness	1	200
iPBP	2	252			
Total	7789g (~2.6% margin left)				

2.4 Payload

Five mission goals of the GOMI SAT mission are elaborated in the Section 1. To accomplish the goals of (1), (2), (4), (5), GOMI SAT CubeSat is equipped with four sensors: a SWIR Camera, a

thermal Camera, a CMOS visible light Camera, and a GNSS-R. The selected models and their specifications are discussed below:

2.4.1 SWIR Camera

The SWIR Camera (Figure 2.4.1) is used to detect microplastics on the ocean surface. According to existing research, microplastics have several absorption lines at the SWIR band. This SWIR Camera has two sets of independent scopes and sensors with different filters to image at different wavelength. The filter wavelengths are programmed at 1215nm and 1120nm respectively. Because microplastics have different reflectance at these two wavelengths, and the reflectance at SWIR band is low. However, the coverage of microplastics is extremely low, so the design needs some calculation to confirm if the sensitivity of the SWIR can satiated the mission goal (2) or not. The specifications of SWIR Camera are showed in Table 4,5,6.

Table 4. The specifications of camera

Name	Wildcat 640 U3V 100
Mass (kg)	0.358
Dimension(mm)	55 × 55 × 91.5
Power(W)	<6
interface	USB3.0
Pixel size(um)	20
Image format (pixels)	640 × 512
Readout noise (e-)	80
Full well capacities (e-)	110k
Quantum efficiency	70%
Spatial resolution	568 m @710km
Swath	727.04 km @710km

Table 5. The specifications of lens

Name	GAOPTICS 25mm SWIR Lenses
Mass (kg)	<0.200
Dimension(mm)	64 × 64 × 56.6

Table 6. The specifications of the filters

Name	SWIR band filter
Mass (kg)	<0.020
Dimension(mm)	30 × 30 × 1
Wavelength	1215 nm and 1010 nm
Bandwidth	30nm

2.4.1.1 SNR of SWIR Camera with different coverage of microplastics

Table 7. symbol definition

Symbol	Meaning
F_{sea}	Irradiation (W m^{-2} nm^{-1}) from the seawater
F_{solar}	Irradiation (W m^{-2} nm^{-1}) from the Sun at sea level
F_{MP}	Irradiation (W m^{-2} nm^{-1}) from the microplastics
α_{sea}	Reflectance of the seawater
α_{atm}	Transparency of the atmosphere

α_{MP}	Reflectance of the microplastics
C_{MP}	Coverage ratio of microplastics
q	J to electron volt
λ	Wavelength (nm)
BW	Bandwidth(nm)
Φ_{sea}	Photon flux ($m^{-2}sec^{-1}$) from seawater
Φ_{MP}	Photon flux ($m^{-2}sec^{-1}$) from microplastics
S_{sea}	Signal from seawater
S_{MP}	Signal from microplastics
N_{total}	Total noise
$N_{readout}$	Readout noise
N_{sea}	Noise from seawater
N_{MP}	Noise from microplastics
D	radius of scope(m)
H	Orbit height(m)
P	Spatial resolution(m)
QE	Quantum efficiency
T	Exposure time(sec)

Since the reflectivity of seawater at these two wavelengths is very low, and the reflectivity of microplastics at 1010nm is 2.4 times as at 1215nm (10% and 24%), the difference in signal strength between the two images obtained by the payload should be caused by the microplastics floating on the sea surface. The next question that needs to be considered is whether the difference in signal strength caused by the microplastics is strong enough to detect and analyze. Move forward, how much coverage of the microplastics on the sea surface needs to be in order to overcome the system noise. We divide into several situations to discuss theoretically the signal and noise intensity that the camera will get. See Table 7 for symbol explanation.

Situation A. Pure seawater, zero microplastics
Radiant intensity reflected by seawater (@orbit 725km)
[for 1215nm] 0.44(W/m^2/nm) * 1% * 90%
= 0.00396 (W/m^2/nm)

[for 1010nm] 0.69(W/m^2/nm) * 1% * 92%
= 0.006348 (W/m^2/nm)
Converted into photon flux

[for 1215nm] $\Phi_{sea} = F_{sea} \times \frac{1}{q} \times \frac{\lambda}{1240} \times BW$

= 0.00396(W/m^2/nm) * 1 / (1.6 *10^-19)(J/eV) * 1215(nm) / (1.24*10^3)(eV*nm) * 30(nm)

= 7.275*10^17(photon/m^2/sec)

[for 1010nm] $\Phi_{sea} = F_{sea} \times \frac{1}{q} \times \frac{\lambda}{1240} \times BW$

= 0.006348 (W/m^2/nm) * 1 / (1.6 *10^-19)(J/eV) * 1010(nm) / (1.24*10^3)(eV*nm) * 30(nm)

= 9.695*10^17 (photon/m^2/sec)

The signal from seawater collected by each pixel

[for 1215nm] $S_{sea} = \Phi_{sea} \times P^2 \times \frac{\pi D^2}{4\pi H^2} \times QE \times T$

= 7.275*10^17(photon/m^2/sec) * 580 (m)^2 * (π*0.008929m^2) / (4π*725000m^2) * 73% * 1(s)

= 6774200 (photon)

[for 1010nm] $S_{sea} = \Phi_{sea} \times P^2 \times \frac{\pi D^2}{4\pi H^2} \times QE \times T$

= 9.695*10^17 (photon/m^2/sec) * 580 (m)^2 * (π*0.008929m^2) / (4π*725000m^2) * 60% * 1(s) = 7419500 (photon)

In the case of 0% microplastic coverage, the signal difference of the two wavelengths (1010nm – 1215nm) is：

7419500 - 6774200 = 645300

Situation B. Seawater and microplastics with 1% coverage

Because 1% of the seawater is covered by microplastics, the seawater signal will be 99% of the situation A. ◦

[for 1215nm] S_{sea} = 6774200 (photon) * 99% = 6706500 (photon)

[for 1010nm] S_{sea} = 7419500 (photon) * 99% = 7345300 (photon)

The signal calculation method of microplastics is similar to the seawater,

Intensity of radiation reflected by microplastics (@orbit 725km)

[for 1215nm] $F_{MP} = F_{solar} \times \alpha_{MP} \times \alpha_{atm} \times C_{MP}$ = 0.44(W/m^2/nm) * 10% * 90% * 1%

= 0.000396 (W/m^2/nm)

[for 1010nm] $F_{MP} = F_{solar} \times \alpha_{MP} \times \alpha_{atm} \times C_{MP}$ = 0.69(W/m^2/nm) * 24% * 92% *1%

= 0.00152 (W/m^2/nm)

Converted into photon flux

[for 1215nm] $\Phi_{MP} = F_{MP} \times \frac{1}{q} \times \frac{\lambda}{1240} \times BW$

= 0.000396 (W/m^2/nm) * 1 / (1.6 *10^-19)(J/eV) * 1215(nm) / (1.24*10^3)(eV*nm) * 30(nm)
= 7.275*10^16 (photon/m^2/sec)

[for 1010nm] $\Phi_{MP} = F_{MP} \times \frac{1}{q} \times \frac{\lambda}{1240} \times BW$

= 0.00152 (W/m^2/nm) * 1 / (1.6 *10^-19)(J/eV) * 1010(nm) / (1.24*10^3)(eV*nm) * 30(nm)
= 2.327*10^17 (photon/m^2/sec)

The signal from microplastics collected by each pixel

[for 1215nm] $S_{MP} = \Phi_{MP} \times P^2 \times \frac{\pi D^2}{4\pi H^2} \times QE \times T$

= 7.275*10^16 (photon/m^2/sec) * 580 (m)^2 * (π*0.008929m^2) / (4π*725000m^2) * 73% * 1(s)
= 677400 (photon)

[for 1010nm] $S_{MP} = \Phi_{MP} \times P^2 \times \frac{\pi D^2}{4\pi H^2} \times QE \times T$

= 2.327*10^17 (photon/m^2/sec) * 580 (m)^2 * (π*0.008929m^2) / (4π*725000m^2) * 60% * 1(s)
= 1781400 (photon)

The signal of the combination of seawater and microplastics are
[for 1215nm] $S_{total} = S_{sea} + S_{MP} = 6706500 + 677400 = 7383900$
[for 1010nm] $S_{total} = S_{sea} + S_{MP} = 7345300 + 1781400 = 9126700$
Noise are

[for 1215nm] $N_{total} = \sqrt{S_{sea}} + \sqrt{S_{MP}} + N_{readout}$

= √6706500 + √677400 + 80 = 3493

[for 1010nm] $N_{total} = \sqrt{S_{sea}} + \sqrt{S_{MP}} + N_{readout}$

= √7345300 + √1781400 + 80 = 4125

Total system noise is
√(3493^2 + 4125^2) = 5405
In the case of 1% microplastic coverage, the signal difference of the two wavelengths(1010nm - 1215nm) is：
9126700 - 7383900= 1742800
Compared to the case of pure seawater, the signal difference between the two wavelengths increases:
1742800 – 645300 = 1097500

Much larger than system noise 5405，SNR is about 10log(1097500/5405) ≒ 23dB
Therefore, when the coverage of microplastics is around 1%, our system can have a good chance of observing the presence of microplastics and has a very high SNR. With an appropriate model should be able to quantify the coverage of microplastics.

Situation C. Seawater and microplastics with 0.01% coverage
Since the coverage rate of microplastics is extremely low, ignoring its influence on the seawater signal, the seawater signal is the same as the Situation A
[for 1215nm] $S_{sea} = 6774200$ (photon)
[for 1010nm] $S_{sea} = 7419500$ (photon)

The signal from Microplastics calculation method is similar to the situation B
Intensity of radiation reflected by microplastics (@orbit 725km)
[for 1215nm] $F_{MP} = F_{solar} \times \alpha_{MP} \times \alpha_{atm} \times C_{MP} = 0.44$(W/m^2/nm) * 10% * 90% * 0.01%
= 0.00000396 (W/m^2/nm)
[for 1010nm] $F_{MP} = F_{solar} \times \alpha_{MP} \times \alpha_{atm} \times C_{MP} = 0.69$(W/m^2/nm) * 24% * 92% * 0.01%
= 0.0000152 (W/m^2/nm)

Converted into photon flux
[for 1215nm] $\Phi_{MP} = F_{MP} \times \frac{1}{q} \times \frac{\lambda}{1240} \times BW$
= 0.00000396 (W/m^2/nm) * 1 / (1.6 *10^-19)(J/eV) * 1215(nm) / (1.24*10^3)(eV*nm) * 30(nm)
= 7.275*10^14 (photon/m^2/sec)
[for 1010nm] $\Phi_{MP} = F_{MP} \times \frac{1}{q} \times \frac{\lambda}{1240} \times BW$
= 0.0000152 (W/m^2/nm) * 1 / (1.6 *10^-19)(J/eV) * 1010(nm) / (1.24*10^3)(eV*nm) * 30(nm)
= 2.327*10^15 (photon/m^2/sec)

The signal from microplastics collected by each pixel
[for 1215nm] $S_{MP} = \Phi_{MP} \times P^2 \times \frac{\pi D^2}{4\pi H^2} \times QE \times T$
= 7.275*10^14 (photon/m^2/sec) * 580 (m)^2 * (π*0.008929m^2) / (4π*725000m^2) * 73% *
1(s) = 6774 (photon)
[for 1010nm] $S_{MP} = \Phi_{MP} \times P^2 \times \frac{\pi D^2}{4\pi H^2} \times QE \times T$
= 2.327*10^15 (photon/m^2/sec) * 580 (m)^2 * (π*0.008929m^2) / (4π*725000m^2) * 60% *
1(s) = 17814 (photon)

The signal of the combination of seawater and microplastics are
[for 1215nm] $S_{total} = S_{sea} + S_{MP} = 6774200 + 6774 = 6780974$

[for 1010nm] $S_{total} = S_{sea} + S_{MP} = 7419500 + 17814 = 7437314$

Noise are

[for 1215nm] $N_{total} = \sqrt{S_{sea}} + \sqrt{S_{MP}} + N_{readout}$

= √6774200 + √6774 + 80 = 2765

[for 1010nm] $N_{total} = \sqrt{S_{sea}} + \sqrt{S_{MP}} + N_{readout}$

= √7419500 + √17814 + 80 = 2937

Total system noise is
√(2765^2 + 2937^2) = 4034
In the case of 0.01% microplastic coverage, the signal difference of the two wavelengths(1010nm - 1215nm) is：
7437314 - 6780974= 656340

Compared to the case of pure seawater, the signal difference between the two wavelengths increases:
656340 – 645300 = 11040

Slightly larger than system noise 4034, SNR is about 10log(11040/4034) ≒ 4.3dB
Therefore, our system can observe the presence of microplastics when the coverage of microplastics is around 0.01%, and the SNR is greater than 3dB.

2.4.2 Thermal Camera

Thermal Camera would measure the temperature of ocean by direct imaging ocean surface. Besides measuring the temperature of ocean, Thermal Camera also provide data helps to detect cloud. The specification of Thermal Camera is showed in Table 8.

Table 8. The specifications of the Thermal Camera

Name	FLIR Boson 640 with 14mm lens
Mass (kg)	0.027
Dimension of Lens (mm)	26 × 26 × 17.5
Dimension of sensor (mm)	29 × 34.5 × 17.5
Power(W)	~0.500
interface	I2C、SPI
Pixel size(um)	12
Image format (pixels)	640 × 512

The spatial resolution is 393m when the camera is placed at 710km height which is smaller than the spatial resolution of the SWIR Camera. It can provide higher resolution images.

2.4.3 CMOS Visible Light Camera

C3D is a TRL 9 CubeSat camera system with proven flight-heritage having flown on both the UK Space Agency's UKube-1 and AlSat Nano missions. It has good reliability. The specification of

CMOS Visible Light Camera is showed in Table 9.

Table 9. The specifications of the CMOS Visible Light Camera

Name	XCAM C3D CubeSat Camera
Mass (kg)	0.085
Dimension (mm)	95 × 91 × 27
Power(W)	< 0.845
interface	I2C、SPI
Pixel size(um)	5.3
Image format (pixels)	1280 × 1024

2.4.4 GNSS-R

The movement of microplastics is highly related to ocean currents and wind fields. Most simulation models also need the speed and direction of currents and winds. Therefore, to measure the currents and winds, GOMI SAT needs specific sensors to obtain the above parameters. However, currents and winds are difficult to measure remotely, and active sensors are favored in previous missions but impractical for CubeSats. Fortunately, GNSS-reflectometry technology becomes mature and stable in recent years. Because GNSS-R is a passive sensor and power consumption is not as high as Radar or Laser, and it is a better sensor for small satellites or CubeSats. The design of GNSS-R onboard the GOMI SAT CubeSats is based on CYGNSS's DDMI, TechDemoSat-1's SGR-ReSI, and PRETTY's SEPP from ESA.

Table 10 The specification of Cyclone V SoC

Name	Cyclone V SoC Board
Mass (kg)	0.1
Dimension (mm)	150x100x15
Power(W)	2.7
interface	UART, CAN, I2C…

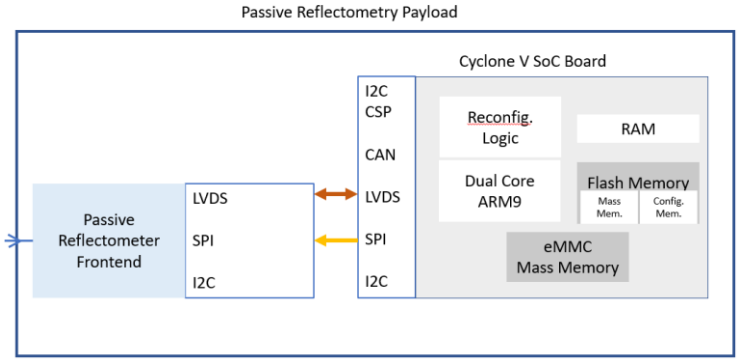

Figure 6. The block diagram of GNSS-R

2.5. The Subsystem of GOMI SAT

2.5.1. SMS

GOMI SAT is designed as a standard 6U CubeSat with all details done according to the rules specified by the contest and the CubeSat Design Specification (CDS), e.g., weighing less than 8 kg per unit, 50 kg in total, and being smaller than 50 cm x 50 cm x 50 cm in size when combined. For each unit, its internal subsystems (Figure 7) are protected by the main structure, including 2 side

plates, several supporters, and a 6U frame. As for coordinate definition, the +Z axis is the nadir direction while the +X axis is the direction GOMI SAT is moving towards.

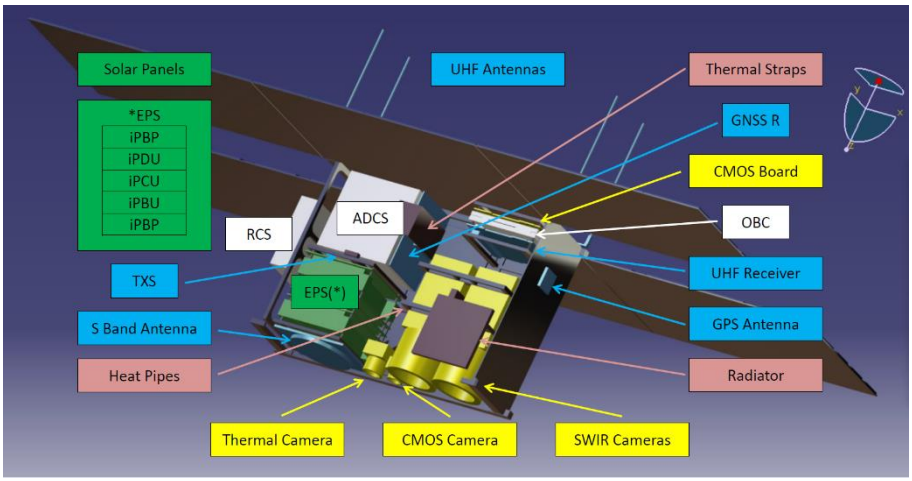

Figure 7. Overview of GOMI SAT's internal layout

2.5.1.1. Structural requirements

GOMI SAT's structure must survive the launch and its entire life cycle, especially the former one. Listed in tables 11 to 14 are data acquired in an H-IIA rocket launch.

Table 11. Quasi-Static Acceleration

	Axis direction	Axis orthogonal direction
Compression	-6.0 G	±5.0 G
Tension	5.0 G	±5.0 G

Table 12. Sine Wave Vibration Levels

Direction	Frequency (Hz)	Acceleration
Longitudinal	5-100	2.5 G
Lateral	5-100	2.0 G

Table 13. Random Vibration Levels.

Frequency Width (Hz)	Acceleration (G^2 /Hz)
20-200	+3 dB/octave
200-2,000	0.032
Actual	7.8Grms

Table 14. Rigidity requirement

Axis direction	Axis orthogonal direction
More than 120 Hz	More than 60 Hz

2.5.1.2. Material

Al-6061-T6 and SUS304 alloys are used in the main structure while FR-4 epoxy builds up the rest of the boards and panels onboard GOMI SAT.

2.5.1.3. Structural analysis

It is important to prove whether GOMI SAT meets its structural requirements or not. With the help of Finite Element Analysis, we can perform tests even before it's manufactured. The process of our analysis is shown in Figure 8.

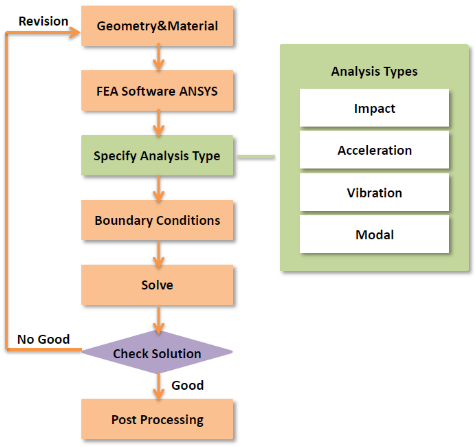

Figure 8. Flowchart of analyzing GOMI SAT's structure and internal layout

ANSYS is used to analyze the structure. The modal analysis aims to acquire the structure's natural frequencies, preventing GOMI SAT to resonance in the frequency given by the rocket. Random vibration is then performed to get the corresponding stress. These are effective ways to analyze fatigue or destruction of the satellite.

2.5.1.3.1. Modal analysis

Table 15 shows 10 modes calculated to find out where GOMI SAT would strongly resonance. The first mode is 232.7 Hz, higher than the required 120 Hz. Figure 9 shows the shape of the deformation under the first resonance mode.

Table 15. First 10 natural frequencies

Mode	Frequency (Hz)	Mode	Frequency (Hz)
1.	232.7	6.	542.32
2.	303.51	7.	549.04
3.	432.94	8.	550.06
4.	479.95	9.	581.
5.	485.41	10.	653.76

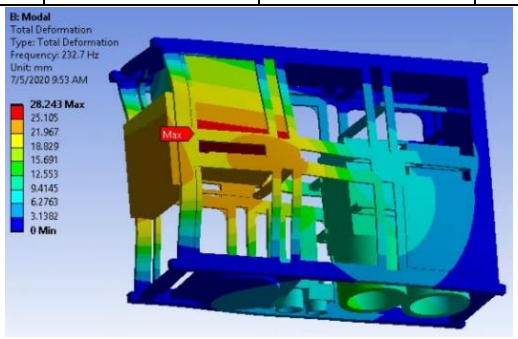

Figure 9. ANSYS modal analysis results of GOMI SAT

2.5.1.3.2. Random vibration analysis

The random vibration analysis may show the response of a system sustaining a external continuous oscillation. Figure 10 shows the maximum stress in 3-σ is 130.75 MPa acting on the aluminum alloy, which is insufficient to cause failures on the structure.

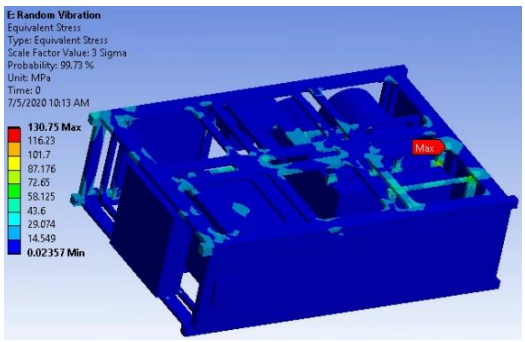

Figure 10. ANSYS random vibration result of GOMI SAT

2.5.1.3.3. Static structural analysis

A static structural analysis is performed to determine the stress on physical components correspond to the loads. Applying a 5G acceleration in the longitudinal direction, the stress distribution is shown in Figure 11.

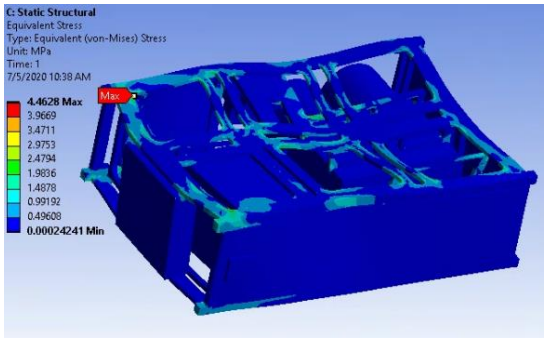

Figure 11. ANSYS static structural analysis result of GOMI SAT

2.5.1.3.4. Harmonic response analysis

The harmonic response analysis is used to check the stress responding to a sine wave load. Applying a 2.5G acceleration across 5-100 Hz, the analysis result is presented in Figure 12.

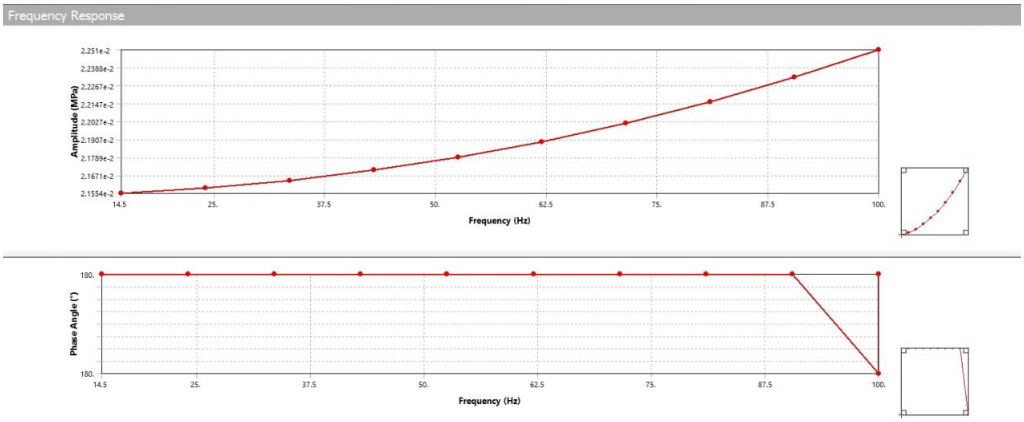

Figure 12. ANSYS harmonic response analysis result of GOMI SAT

2.5.2 TCS

The thermal control system is designed to confirm that all systems in GOMI can withstand the thermal condition in orbit.

2.5.2.1. Thermal Control Design

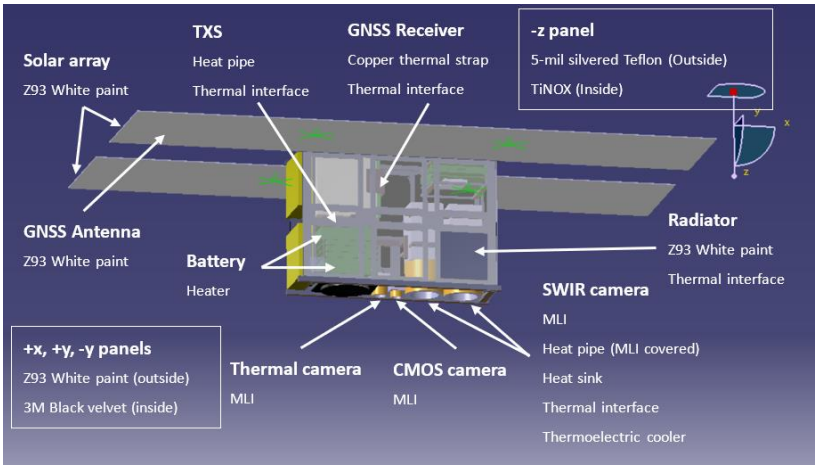

Figure 13. TCS design of GOMI-SAT

The goal of thermal control design is to maintain each component in their preferred temperature range both when in operation and in storage conditions. The thermal control design layout can be shown in Figure 13. GOMI-SAT uses passive thermal control approaches to the maximum extents and active thermal controls at the remote-sensing payload.

Table 16 Thermal treatments

Element	Thermal Treatment
+x, +y, -y panels	Z93 White paint (outside)
	3M Black velvet (inside)
-z panel	5-mil silvered Teflon (outside)
	TiNOX (inside)
Solar Array	Z93 White paint
Radiator	Z93 White paint (outside)
	Thermal interface, CHO-THERM 1671
	MLI, Black Kapton (inside)
Battery	Heater
TXS	Passive heat pipe, Freon R-113 working fluid
	Thermal interface, CHO-THERM 1671
GNSS Receiver	Copper thermal strap
	Thermal interface, CHO-THERM 1671
GNSS antenna	Z93 White paint
SWIR camera	Thermoelectric (TE) cooler
	Passive heat pipe, Freon R-11 working fluid, Black Kapton MLI covered
	Heat sink, Copper
	Thermal interface, CHO-THERM 1671
	MLI, Aluminized Kapton based
Thermal camera	MLI, Aluminized Kapton based
CMOS camera	MLI, Aluminized Kapton based

2.5.2.2. Requirements relative to Thermal Control

2.5.2.2.1 Temperature

The operating and storage temperature ranges and the heat dissipation of GOMI-Sat components are listed in Table 17 respectively.

Table 17 Satellite design temperature

Product Reference	Operating temperature (℃)		Storage temperature (℃)		Heat dissipation(W)
Bus					
Structure subsystem (SMS)					
Structure	-40	80	-40	80	0
Electrical and Power Subsystem (EPS)					
iPCU	-40	70	-40	85	0.397
iPBU	-40	70	-40	85	0.063
iPBP	-40	70	-40	85	45
iPDU	-40	70	-40	85	0.066
On Board Data Handling Subsystem (OBC)					
iOBC	-25	65	-40	80	1
Attitude Determination and Control Subsystem (ADCS)					
XACT-50	-20	60	N/A	N/A	6
MEPSI	0	60	N/A	N/A	0
Communication Board (COM)					
TXS	-40	70	-40	70	13
S-band Ant.	-40	85	-40	85	2
NanoCom AX-100	-30	85	-30	85	1
NanoCom Ant-6f UHF	-40	85	-40	85	3
Payload					
SWIR	-40	70	-40	85	6
CMOS Camera	-25	65	-35	70	0.845
Thermal Camera	-40	80	-50	105	0.5
GNSS Reflectometer	-40	85	-40	85	2.7

Additional requirement: The CCD in the SWIR camera should be kept below 15℃ during operation to achieve optimal performance when GOMI-Sat is at payload mode, due to the increase in dark current as of the temperature increases (doubles every 6~7℃).

2.5.2.2.2 Temperature margin

Taking errors and uncertainties on the thermo-physical properties into account, a thermal uncertainty margin of 10°C is applied on all the yielded values for all passive-controlled units, and a thermal uncertainty margin of 2°C is applied on all the computed values for all active-controlled units.

2.5.2.2.3 Life duration

The life duration of the satellite is of 10 years and affects the thermo-physical properties of the external coating.

2.5.2.2.4 Orbital Environment and Spacecraft attitude

The orbital environment considered for the cold and hot thermal cases are reported in Table 18. The table that shade in gray are the applied condition.

Table 18 Orbital environments

			Env1	Env2
Case	Hot			
	Cold			
Altitude (km)		725		
Inclination (deg.)		98.30		
Orbital Env.	Solar constant (W/m²)	1412.0		
		1321.0		
	Earth emission (W/m²)	214		
		231		
	Albedo coeff.	0.28		
		0.16		

2.5.2.2.5 Power dissipation of components

The Table 19 list the duty cycle and heat dissipation of every equipment in each orbit during the nominal flight mode. There are four phases in an orbit, which means that GOMI-SAT will change the flight mode three times in an orbit.

Table 19 Power dissipation in nominal flight mode in an orbit

	Phase Number	1	2	3	4
Nominal	Start (s)	0	3850	4226	5581
	End (s)	3850	4226	5581	5958
	Duration (s)	3850	376	1355	377
	Duty cycle	64.6%	6.3%	22.8%	6.3%
Phase	Payload Mode				
	Stand-By Mode				
	Communication Mode				
SMS	Structure	0	0	0	0
EPS	iPCU	0.397	0	0	0
	iPBU	0.063	0.063	0.063	0.063
	iPBP	0	45	45	45
	iPDU	0.066	0.066	0.066	0.066
OBC	iOBC	1	1	1	1
ADCS	XACT-50	6	1*	6	1*
	MEPSI	0	0	0	0

COM	TXS	0	0	13	0
	S-band Ant.	0	0	2	0
	NanoCom AX-100	0	0	1	0
	NanoCom Ant-6f UHF	0	0	3	0
Payload	SWIR_1	6	0	0	0
	SWIR_2	6	0	0	0
	CMOS Camera	0.845	0	0	0
	Thermal Camera	0.5	0	0	0
	GNSS Reflectometer	2.7	0	0	0
Total		24.571	47.129	80.129	47.129

*When in stand-by mode, the XACT-50 will have a lower power consumption, so the heat dissipation is lower too.

2.5.2.3. Thermal Analysis

The thermal analysis is calculated by ANSYS Transient Thermal modulus, which utilizes the Finite Element method.

2.5.2.3.1 Thermo-Physical Properties

Table 20 Solid material thermal properties

Material	ρ (kg/cm^3)	k (W/cm°C)	C_p (W-hr/kg°C)
Al-6061-T6	0.00277	1.679	0.267
Stainless steel 304	0.00803	0.163	0.140
Copper	0.00895	3.86	0.106

Table 21 Thermal interface thermal properties

Thermal Interface	Thermal Impedance (°C-cm²/W) @300psi	k (W/cm°C)	C_p (W-hr/kg°C)	κ (ppm/K)
Cho-therm 1671	1.48	0.026	0.28	250

Table 22 Working fluid thermal properties

Fluid	Melting point (K)	Boiling point (K)	Critical temp. (K)	Operation temp. (K)	Latent heat of vaporization (kJ/mol)
Freon R-113	236.8	320.8	470	260 – 380	25.34
Freon R-11	162.2	297.1	471.2	230 – 400	27.04

Table 23 Surface finish thermal properties

Surface finish	BOL	EOL	BOL	EOL
	ε-Emittance		α-Absorptance	
Z93 White Paint	0.92	0.92	0.18	0.55
3M Black Velvet	0.91	0.84	0.97	0.97
5-mil silvered Telflon	0.78	N/A	0.09	N/A
TiNOX	0.05	N/A	0.95	N/A

2.5.2.3.3 Analysis Cases

For analysis cases, two extreme cases are considered, the worst hot case and the worst cold cases. The worst hot case occurs when GOMI-Sat is placed at the aphelion and in nominal modes. For

the worst cold case, it occurs at the perihelion and in phoenix mode.

2.5.2.3.4 Analysis Result

From the analysis result of the hot and cold cases, the thermal control design of the GOMI-Sat is confirmed to the GOMI-SAT can operate in the thermal condition on its programmed orbit.

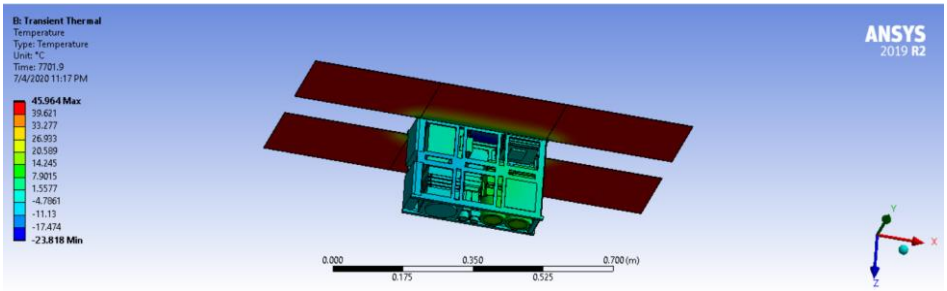

Figure 14. Hot Case of GOMI

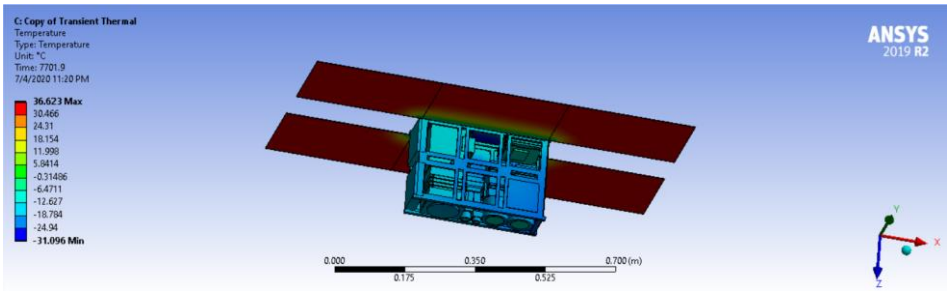

Figure 15. Cold Case of GOMI

Table 24 Analysis Result

		Hot case		Cold case	
	Component	Tmax(℃)	Tmin(℃)	Tmax(℃)	Tmin(℃)
SMS	Structure	13.49	-4.32	-9.72	-19.17
EPS	iPCU	0.84	-3.29	-13.04	-14.99
	iPBU	1.43	-3.64	-12.55	-13.94
	iPBP	2.43	-4.59	-15.97	-17.88
	iPDU	2.35	-3.59	-12.83	-14.39
OBC	iOBC	5.16	-5.55	-5.14	-9.98
ADCS	XACT-50	5.77	-7.40	-12.06	-21.15
	MEPSI	3.63	-6.10	-11.31	-19.91
COM	TXS	25.06	-8.08	-15.95	-20.81
	S-band Ant.	-0.30	-10.80	-17.46	-22.07
	NanoCom AX-100	24.32	-5.15	-7.75	-16.58
	NanoCom Ant-6f UHF	6.06	-9.10	-10.7	-22.23
Payload	SWIR_1	13.08	-6.80	-19.8	-22.81
	SWIR_2	12.737	-6.67	-19.71	-22.94
	CMOS Camera	1.86	-6.57	-18.56	-21.304
	Thermal Camera	1.41	-6.03	-18.14	-20.83
	GNSS-R	7.92	-5.59	-12.16	-20.308

2.5.3 Attitude Determination and Control System (ADCS)

2.5.3.1 ADCS overview

The task of the GOMI SAT is to take images over oceans. The satellite attitude control is critical to such imaging mission, and it must be carefully considered. The field of view of GOMI SAT is 29° ×22°. Assuming that the adjacent images may have 5% overlap. Then the target of the view is 0.55° and the pointing accuracy is one-tenth of target of view, which is about 0.05°. The camera on GOMI SAT aims nadir direction for best observing quality. Zero momentum bias control method is conducted, which has an accuracy of +/- 0.001° and meet our requirement. Attitude sensors like star tracker, sun sensor and magnetometer are employed to provide information of satellite attitude. Actuators like reaction wheels and torque rods are used to control GOMI SAT. The specification of ADCS capability are listed in Table 25.

Table 25 Specification of XACT-50 [6]

	XACT-50
Mass (kg)	1.23
Dimension (cm^3)	10 × 10 × 7.54
Power (W)	1~3
Pointing Accuracy	$\pm 0.003^{\circ}$ for 2 axes $\pm 0.007^{\circ}$ for 3rd axis
Pointing Acknowledge	+/- 0.06 arcminutes
Input Voltage (V)	12
Slew Rate	$\geq 10\,\mathrm{deg/sec}$
Momentum (Nms)	0.05
Interface	RS-422
Operating Temperature ($°C$)	-20~60
TRL	9

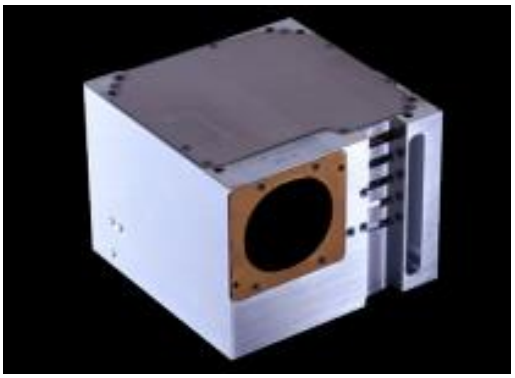

2.5.3.2 Disturbance Torque Quantification

To accurately control the attitude of the GOMI SAT CubeSats, a disturbance environment must be defined first to choose appropriate actuators. There are four major external disturbance torques: solar radiation pressure (SRP), atmospheric drag, magnetic field, and gravity gradient [7]. These disturbances are estimated later.

- Solar Radiation Pressure (SRP)

  The SRP can be presented as equation (2.5.1)

$$T_S = \frac{\phi}{c} A_s (1+q)(cp_s - cm)\cos\varphi \tag{2.5.1}$$

Table 26 Parameters in equation (2.5.1)

ϕ	Solar constant $(=1367 W/m^2)$
c	Speed of light $(=3\times10^8\ m/s)$

A_s	Sunlit surface area (m^2)
q	Reflectance constant $(=0.6)$
cp_s	Center of pressure (m^2)
cm	Center of mass (m^2)
φ	Max. angle of incidence of sun $(=0^\circ)$

- Atmospheric Drag

  The atmospheric drag can be presented as equation (2.5.2)

$$T_a = \frac{1}{2}\rho C_d A_r V^2 (cp_a - cm) \tag{2.5.2}$$

Table 27 Parameters in equation (2.5.2)

ρ	Atmospheric density $(=10^{-13}\, kg/m^3)$
C_d	Drag coefficient $(=2.5)$
A_r	Ram area (m^2)
V	Orbital velocity (m/s)
cp_a	Center of aerodynamic pressure (m)

- Magnetic Field

  The disturbance of magnetic field can be presented as equation (2.5.3)

$$T_m = m \cdot B \tag{2.5.3}$$

Table 28 Parameters in equation (2.5.3)

m	Residual dipole moment $(A \cdot m^2)$
B	Magnetic field strength (T)

- Gravity Gradient

  The disturbance of gravity gradient can be presented as equation (2.5.4)

$$T_g = \frac{3\mu}{2R^3}\left|I_z - I_y\right|\sin(2\theta) \tag{2.5.4}$$

Table 29 Parameters in equation (2.5.4)

μ	Gravitational constant $(=3.986\times10^{14}\, m^3/s^2)$
R	Distance from center of earth (m)
I_z, I_y	Moment of inertia about Y and Z axis $(kg \cdot m^2)$
θ	Angle between vertical and Z axis

According to equation (2.5.1) to (2.5.4), the total disturbance torque T_d can be calculated, and yields as (2.5.5). Appropriate actuators can be chosen, and attitude control simulation is conducted later.

$$T_d = 1.833\times10^{-6}(N \cdot m) \tag{2.5.5}$$

2.5.3.3 Satellite Attitude Control Simulation

The figure 16 shows the block diagram of satellite dynamic simulation. After satellite separation from rocket, torque rods are used for detumbling.

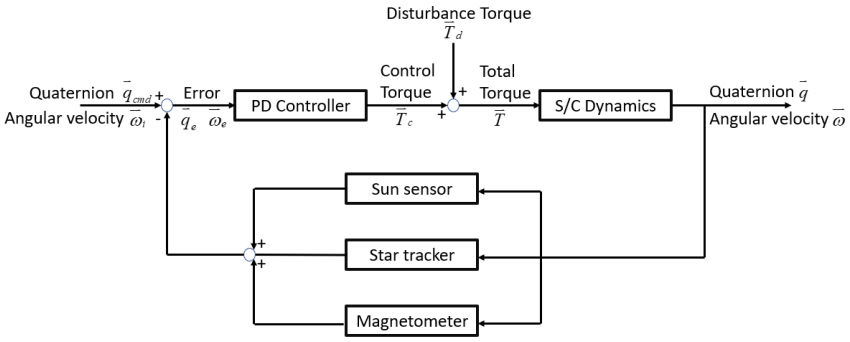

Figure 16. Block diagram of satellite dynamic

While GOMI SAT operates in the orbit, there's still some regions unable to be observed if the CubeSats always keep nadir direction. Ground station should command the CubeSats to adjust its attitude for the best coverage. The dynamics of the GOMI SAT CubeSats can be derived from equation (2.5.6) [8].

$$J\dot{\vec{\omega}}_{b/i} = \vec{T}_c + \vec{T}_d - \vec{\omega}_{b/i} \times (J\vec{\omega}_{b/i} + \vec{h}_w) - \dot{\vec{h}}_w \tag{2.5.6}$$

where $\vec{T}_c$ is the applied magnetorquer control and momentum wheel control, $\vec{\omega}_{b/i}$ is the body angular velocity in ECI frame. Satellite attitude can be defined by quaternions as:

$$\vec{q} = \begin{bmatrix} q_1 & q_2 & q_3 & q_4 \end{bmatrix}^{\mathrm{T}} \tag{2.5.7}$$

where $\vec{q}_1$, $\vec{q}_2$, $\vec{q}_3$ is the rotation about three axis and $\vec{q}_4$ is the translation of satellite. Assuming the initial condition of quaternion is $\vec{q} = \begin{bmatrix} 0 & 0.7071 & 0 & 0.7071 \end{bmatrix}^{\mathrm{T}}$ while GOMI SAT operates without attitude control yet. Based on attitude error, a controller in equation (2.5.8) can be designed using linear control laws [9].

$$v = -K_1(q - q_d) - K_2\dot{q} \tag{2.5.8}$$

where v is the control input to eliminate the attitude error, $\vec{q}_d$ is the desired quaternion. The coefficients K_1 and K_2 are positive constant matrices and they can be determined using linear quadratic regulator method.

Taking the worst case into account, GOMI SAT CubeSats has to rotate 30 degrees along the x-axis to obtain the best coverage. The desired quaternion is $\vec{q}_d = \begin{bmatrix} 0.2588 & 0 & 0 & 0.9659 \end{bmatrix}^{\mathrm{T}}$. Figure 17 shows the angular velocity and attitude of the satellite for a typical slew maneuver.

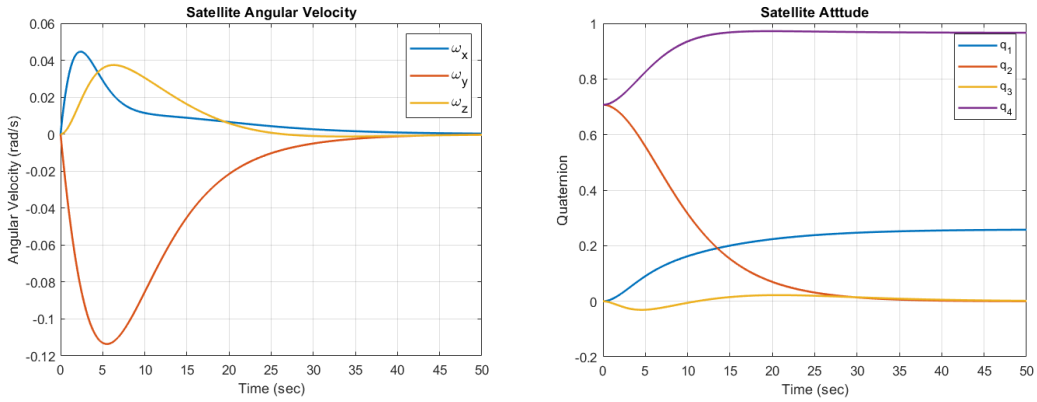

Figure 17. Satellite is settled down in 45 seconds

From the result of dynamics of GOMI SAT, it needs additional 30 seconds to adjust to its desired attitude before it receives commands from ground station or transmits data to ground station. Moreover, **XACT-50 can satisfy the requirement of its mission maneuver.**

2.5.3.4 RCS

The main goal of the propulsion system of GOMI SAT is to perform drag compensation or so-called orbit station keeping. The altitude of GOMI SAT constellation is 725 km altitude, which is almost air-free. The requirement of the propulsion system is low delta-V with low weight, small size, low power consumption, and low thrust. Delta-V requirement is extremely low at 725 km altitude, about 0.5 m/s per year. The chemical propulsion system will cause overheating problems on other components and high delta-V performance of Ion thruster is not necessary. The GOMI SAT CubeSat adopts cold gas propulsion system as its engine, which is relatively simple and stable. MEMS PicoSat Inspector (MEPSI) Micro-Propulsion System (MiPS) is selected as the propulsion system due to low mass, small size, and low delta-V requirement. GOMI SAT is equipped with one MEPSI on each CubeSat, 8.8 m/s total delta-V is provided, which meets the requirement of 5 m/s delta-V for a 10-year station keeping. This propulsion system includes propellant storage, pressurization, distribution, and thrusters. This simple, highly integrated design uses a self-pressurizing liquid propellant that is expelled as a gas. The selected specifications of MEPSI are listed in Table 30.

Table 30. Specifications of MEPSI Micro-Propulsion System

Thrust (mN)	65
$I_{sp}(s)$	65
Total impulse $(N \cdot s)$	34
Dimension (mm^3)	91 × 91 × 25
Dry Mass (g)	456
Propellant Mass (g)	106 (liquid butane)

2.5.4 TT&C

The GOMI SAT CubeSat communicates with the ground station through the TT&C subsystem at two bandpassess: a UHF amateur radio band and a S-band, which uses UHF band Telemetry, tracking and command ground station in National Cheng Kung University and a S-band Telemetry,

tracking and command system operated by the National Space Organization, Taiwan respectively. The UHF amateur radio band use 430-440 MHz to uplink the real-time and time-tagged commands for the mission operation, and the S-band use 2200-2290 MHz to downlink large amount of image data acquired by the payload.

From the calculation by STK, our satellite can cover 22.87% area of global ocean by a single CubeSat, which is equivalent to ~8278940 km^2. The estimation of daily data volume acquired by the payload is summarized in Table 31.

Table 31 Daily data volume

Sensors	Sampling rate	Image size	Daily Volume
Payload			
SWIR camera	783*2 img/day	655360 bits/img	1026 Mbits/day
Thermal camera	783 img/day	655360 bits/img	513 Mbit/day
GNSS-R	57750 sec/day	4096 bits/sec	236.5 Mbit/day
Information			
ADCS	1/30 sec	224 bits	645120 bits/day
Status of Health (SOH)	1/30 sec	2048 bits	58988240 bits/day
Time-Position-Altitude (TPA)	1/30 sec	96 bits	276480 bits/day

Learning from Table 31, the daily data volume is about 1835 Mbits. It is estimated by STK that there are approximate 1040 seconds per day for communication. Thus, the TT&C should provide a data rate of at least 1.8 Mbits per second. Therefore, the data rate of the TT&C is set to 2 Mbits per second.

Modules of GOM SAT AX100 and NanoCom ANT-6F are used as the components of the TT&C receiver in this mission. Furthermore, a ISIS High Data-rate S-band Transmitter and a ISIS S-band patch antenna are employed as the transmitter module. The calculation of the TT&C link budget is listed below:

Table 32 Uplink Budget

Uplink Command Budget:		
Parameter:	*Value:*	*Units:*
Ground Station:		
Ground Station Transmitter Power Output:	10.0	watts
In dBW:	10.0	dBW
In dBm:	40.0	dBm
Ground Stn. Total Transmission Line Losses:	3.6	dB
Antenna Gain:	12.7	dBi
Ground Station EIRP:	19.1	dBW
Uplink Path:		
Ground Station Antenna Pointing Loss:	2.2	dB
Gnd-to-S/C Antenna Polarization Losses:	0.1	dB
Path Loss:	153.6	dB
Atmospheric Losses:	2.1	dB
Ionospheric Losses:	0.4	dB
Rain Losses:	0.0	dB
Isotropic Signal Level at Spacecraft:	-139.3	dBW
Spacecraft (Eb/No Method):		
------- Eb/No Method -------		

Spacecraft Antenna Pointing Loss:	3.0	dB
Spacecraft Antenna Gain:	2.2	dBi
Spacecraft Total Transmission Line Losses:	1.9	dB
Spacecraft Effective Noise Temperature:	463	K
Spacecraft Figure of Merit (G/T):	-26.4	dB/K
S/C Signal-to-Noise Power Density (S/No):	60	dBHz
System Desired Data Rate:	9600	bps
In dBHz:	39.8	dBHz
Command System Eb/No:	20.1	dB
Demodulation Method Seleted:	**GMSK**	
Forward Error Correction Coding Used:	**None**	
System Allowed or Specified Bit-Error-Rate:	1.0E-05	
Demodulator Implementation Loss:	1.0	dB
Telemetry System Required Eb/No:	9.6	dB
Eb/No Threshold:	10.6	dB
System Link Margin:	**9.5**	dB

Table 33 Downlink Budget

Downlink Telemetry Budget:		
Parameter:	*Value:*	*Units:*
Spacecraft:		
Spacecraft Transmitter Power Output:	2.0	watts
In dBW:	3.0	dBW
In dBm:	33.0	dBm
Spacecraft Total Transmission Line Losses:	2.2	dB
Spacecraft Antenna Gain:	6.5	dBi
Spacecraft EIRP:	7.3	dBW
Downlink Path:		
Spacecraft Antenna Pointing Loss:	3.0	dB
S/C-to-Ground Antenna Polarization Loss:	0.0	dB
Path Loss:	168.0	dB
Atmospheric Loss:	2.1	dB
Ionospheric Loss:	0.1	dB
Rain Loss:	0.0	dB
Isotropic Signal Level at Ground Station:	-165.9	dBW
Ground Station (EbNo Method):		
------- Eb/No Method -------		
Ground Station Antenna Pointing Loss:	0.1	dB
Ground Station Antenna Gain:	42.6	dBi
Ground Station Total Transmission Line Losses:	2.0	dB
Ground Station Effective Noise Temperature:	511	K
Ground Station Figure of Merrit (G/T):	13.6	dB/K
G.S. Signal-to-Noise Power Density (S/No):	76.2	dBHz
System Desired Data Rate:	2000000	bps
In dBHz:	63.0	dBHz
Telemetry System Eb/No for the Downlink:	13.2	dB
Demodulation Method Seleted:	**BPSK**	
Forward Error Correction Coding Used:	**Conv. R=1/2,K=7 & R.S. (255,223)**	
System Allowed or Specified Bit-Error-Rate:	1.0E-06	
Demodulator Implementation Loss:	1	dB
Telemetry System Required Eb/No:	2.5	dB
Eb/No Threshold:	3.5	dB
System Link Margin:	**9.7**	dB

The link budget tables of the uplink and downlink between the GOMI SAT and ground station shown above are calculated in the worst case. The longest distance of communication between GOMI SAT and ground station is set as 2619.5 km when the elevation angle is assumed at 5°.

According to the link budget, both uplink and downlink system have enough link margin to handle our mission requirement.

2.5.5 C&DH

Command and Data Handling (C&DH) subsystem

The command and data handling subsystem is the core of the whole satellite. It is designed for our satellite control. The C&DH subsystem consists of the following elements:

1. OBC (On-Board Computer) is an ISIS onboard computer, which has a powerful, efficient, 400 MHz 32-bit ARM9 processor. This OBC has been used in several CubeSat missions, such as providing power and data interface to the payload and ADCS subsystem on a 3U CubeSat PicSat, so it is reliable and suitable for this mission. There are also two redundant Real Time Clocks (RTC) and an external watchdog timer, which is used to reset CPU when it fails, on the board.
2. On-board software includes the onboard hardware abstraction layer library which supports many interfaces such as UART, I2C, SPI, USB and so on. I2C is used to connect with peripheral sensors and some of the subsystems. UART is used to connect with another board for ADCS and GNSS-R. USB is used to connect with payload to control its performance. SPI is used to transfer the data to the memory.
3. DS (Data storage) stores the science data collected from payload and satellite health telemetry. DS has a memory capacity of two 4 GB SD cards with CRC protection.
4. Power Control Unit (PCU) controls the Power Distribution Unit (iPDU) to supply sufficient power to subsystem in different flight modes.
5. Survival Unit (SU) is the continuous power supply to C&DH only and it is independent of EPS. SU provides the minimum required power of the C&DH.

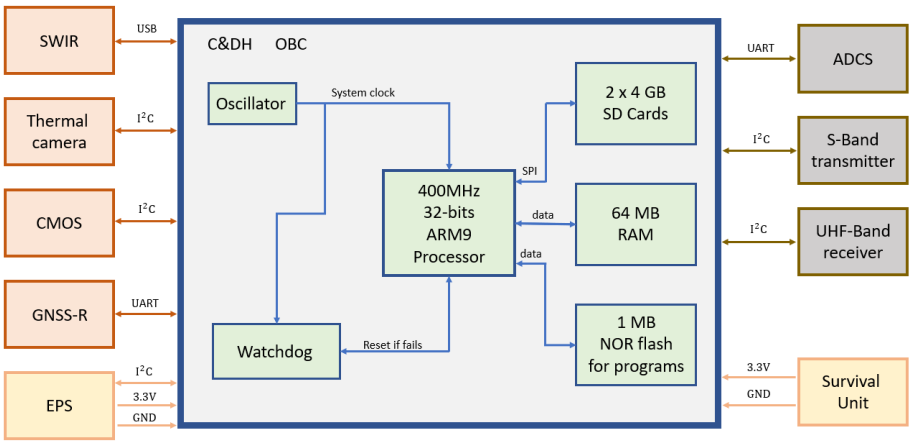

Figure 18. C&DH block diagram

The functions of C&DH are listed and described below:

- Monitoring each subsystem and payload
  - Continuously monitor the condition of each subsystem and payload. Take emergent action if necessary.
- Sending commands to each subsystem
  - C&DH will decide which flight mode to select and send commands to the corresponding

subsystem to operate including sending commands to PDU (power distribution unit) to supply power to these subsystems.

- Collecting data from each subsystem and payload
  - Each subsystem will continuously send their condition data to C&DH and C&DH will store them in data storage waiting for transmission to earth as health report.
  - When the SWIR camera is operating, the science data acquired from it will be processed by AI recognition system. Then, the processed data will be stored in data storage.
  - Data acquired by other payload is also stored in data storage in a formatted form.
- Communicating with ground
  - Carry out the command received from ground.
  - Encode on-board data into specific communication format for transmission to ground.
- Masking data
  - Artificial Intelligence Recognition system (AIRs) will mask the pixels covered by clouds. In this way, the compression ratio can be improved.

Operational processes:

The GOMI SAT CubeSat is programmed with seven operation modes, including phoenix mode, standby mode, payload mode, communication mode, propulsion mode, detumbling mode and safe mode.

Table 34 Flight Mode

Operation Mode	Description
Detumbling Mode	GOMI SAT turns on the OBC and starts to detumble with ADCS.
Safe Mode	GOMI SAT unfolds the solar panels and starts to check all subsystems without malfunction by turns. After all inspections, it sends the health report to the ground station and waits for further commands.
Stand-By Mode	GOMI SAT stands by with only C&DH and EPS on.
Communication Mode	GOMI SAT starts to communicate with the ground, including transmitting the science data and health report of each subsystem to the ground station and receiving the data from the ground station.
Payload Mode	GOMI SAT starts to collect the science data as well as storing them in the data storage.
Propulsion Mode	GOMI SAT turns on the propulsion system and executes the station keeping.
Phoenix Mode	GOMI SAT stops all instruments except OBC which remains the lowest power consumption. The only power supply is the Survival Unit.

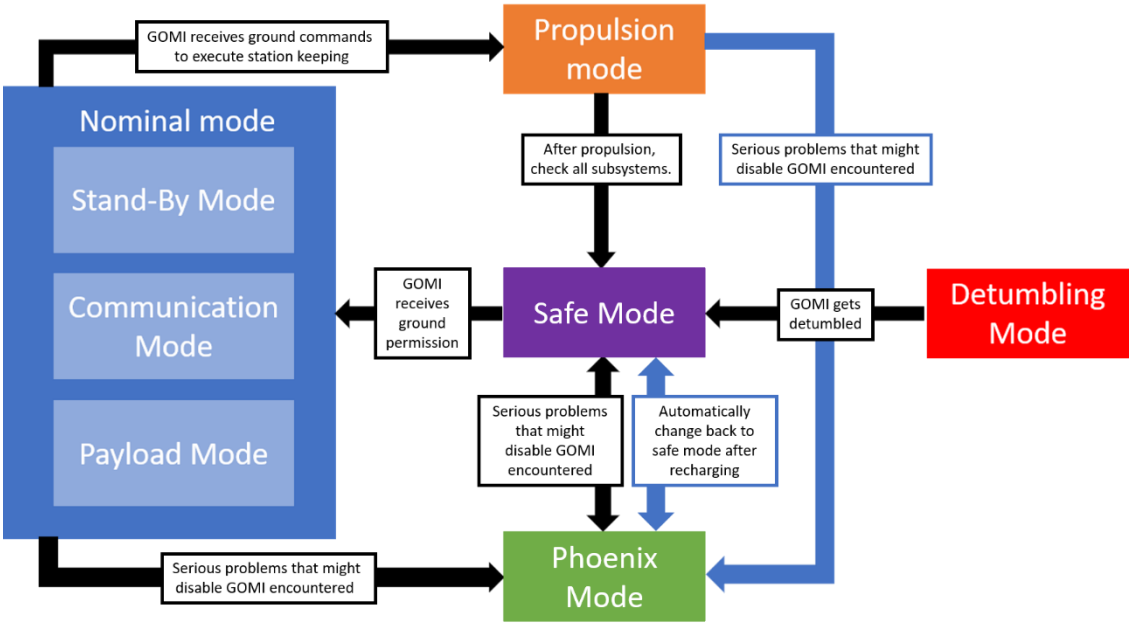

Figure 19. The flowchart of the GOMI SAT operation modes

After the separation from the H-IIA launcher, GOMI SAT enters the Detumbling Mode. OBC is turned on and ADCS is activated to detumble the satellite.

Once GOMI SAT gets detumbled, GOMI SAT enters the Safe Mode automatically. The solar panels are unfolded to ensure the power supply at the beginning of Safe Mode. Then, OBC sends commands to each subsystem and make sure that all subsystem run normally by turns. After all inspections, the health report is sent to the ground station and the CubeSat waits for further commands.

After receiving the health report of GOMI SAT, the ground station sends commands to the GOMI SAT and formally start to acquire science data.

In general, GOMI SAT can operate by itself at this moment. GOMI SAT will periodically change the operation between Payload, Communication, and Standby Modes. GOMI SAT can operate payload to acquire science data in Payload Mode, transmit science data to the ground and receive commands from the ground in the Communication Mode, and otherwise stand by in the Standby Mode.

Due to the drag applied to the satellite, GOMI SAT needs to compensate this factor to maintain the altitude. Thus, propulsion mode begins whenever the attitude is pushing the payload to the edge of malfunction. The thruster is activated as well as ADCS in the Propulsion Mode.

The Phoenix Mode is designed in the case of contingency. Whenever GOMI SAT encounters serious problems, it enters Phoenix Mode autonomously. In this situation, reducing the power consumption of the satellite is the first priority. Thus, GOMI SAT turns off all unnecessary modules and maintains the minimum power consumption. The only running module is OBC, whose power is supplied by Survival Unit. Until the problem is identified and solved, the GOMI SAT will automatically change back to Safe Mode, sending the health report to the ground station and wait for further commands.

Artificial Intelligence Recognition system (AIRs)

For remote sensing, the cloud is an important challenge for acquiring earth's surface data, especially wave detecting at infrared band. Considering clouds with an optical depth larger than 2, approximate 56% of the global surface is covered by clouds. Thus, developing a system to detect clouds and filter the invalid data is able to reduce a considerable amount of invalid data transmitted and decrease the bandwidth for transmission.

To accomplish the goal of cloud detection, the AIRs is designed based on deep learning. Using the data extracted from existing satellite missions, the AIRs can be trained at the ground in advance. Figure 20 shows the flowchart of the cloud detection in AIRs. The details for the cloud detection method is discussed below.

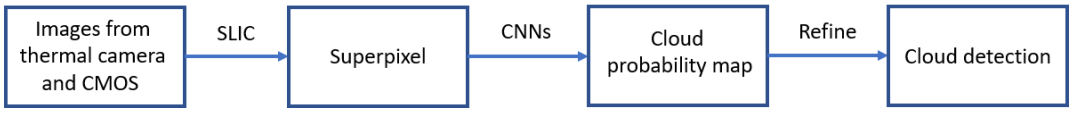

Figure 20. AIRs structure

First, the original images with cloud can be divided into superpixels applying Simple Linear Iterative Clustering (SLIC) algorithm proposed in [10]. Using superpixels as the basic to train can shrink the required time and avoid fragmented noise.

The clustering begins with setting k centers, C_i, of superpixels with interval of S. The following parameters are defined in the CIELAB color space.

$$C_i = \begin{bmatrix} l_i & a_i & b_i & x_i & y_i \end{bmatrix}^{\mathrm{T}}, \quad for\ i = [1, k] \tag{2.5.9}$$

$$S = \sqrt{\frac{N}{k}} \tag{2.5.10}$$

Table 35 Parameters in equation (2.5.9) and (2.5.10)

N	Number of pixels
k	Number of superpixels
S	Distance between two centers of superpixels
(l_i, a_i, b_i)	Color of superpixel i
(x_i, y_i)	Location of superpixel i

After initiating the centers, the distance D, which determines the nearest cluster center for each pixel, is defined as,

$$d_{lab} = \sqrt{(l_j - l_i)^2 + (a_j - a_i)^2 + (b_j - b_i)^2} \tag{2.5.11}$$

$$d_{xy} = \sqrt{(x_j - x_i)^2 + (y_j - y_i)^2} \tag{2.5.12}$$

$$D = \sqrt{{d_{lab}}^2 + (\frac{d_{xy}}{S})^2 m^2} \tag{2.5.13}$$

Table 36 Parameters in equation (2.5.11), (2.5.12) and (2.5.13)

(l_j, a_j, b_j)	Color of pixel j
(x_j, y_j)	Location of pixel
m	Weight to adjust the importance between color similarity and spatial proximity

Using the above definitions, the superpixels can be established. Notice that SLIC only computes distances in a 2S×2S region for each patch.

Second, to generate the map of cloud probability, Convolutional Neural Networks (CNNs) is trained to classify image patches as cloud class or non-cloud class. Since fixed patches used to be the input of CNNs are required, the center pixel of each superpixel is used to represent the patch. Figure 21 is the architecture of the CNNs. It has 4 Convolutional layers (Conv) and 2 Fully Connected layers (FC). To classify cloud or non-cloud class, the last FC has only 2 Neurons and the threshold of determining if the patch covered by cloud is set at 0.5.

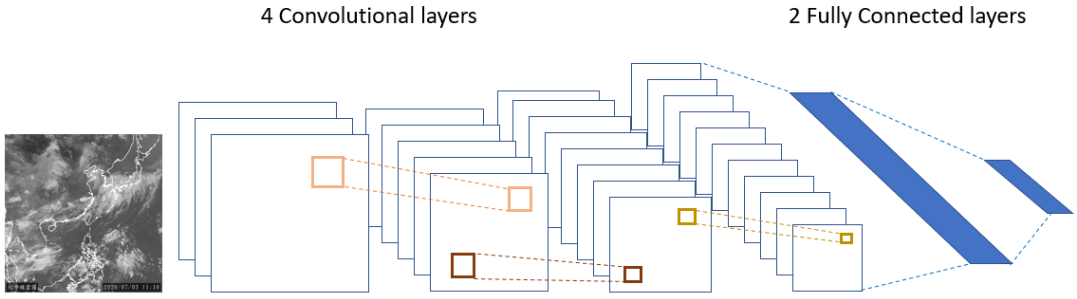

Figure 21. CNNs structure

Third, to reduce the false detection of non-cloud region, especially at the boundary, the cloud probability map is refined using the following equation in [11].

$$gra_a = \begin{cases} Min(pro_1 - pro, ..., pro_m - pro), m > 0 \\ 1 - pro, \qquad\qquad\qquad m = 0 \end{cases} \tag{2.5.14}$$

Table 37 Parameters in equation (2.5.14)

gra_a	Gradient of the superpixel a
pro	Cloud probability of the superpixel a
m	Number of super pixels which have higher probability than a
pro_i	Cloud probability of near superpixels which have higher probability than a

The gradient means the decreasing rate of near superpixels. Setting the threshold $t = 0.3$ to refine the cloud probability map. If the gra_a is higher than t, it is not covered by cloud.

The data from CMOS and thermal camera will be the input of AIRs.

In case of wrong determination, the pixel is determined invalid only when both results of the two images about that pixel are classified into cloud class.

Knowing the location of the invalid pixel, we can mask invalid data in images of SWIR camera

by replacing the pixel data with 0. Thus, with the lossless image compression algorithm JEPG-LS, the more cloud covered in the image, the larger amount of the invalid data transmitted is reduced.

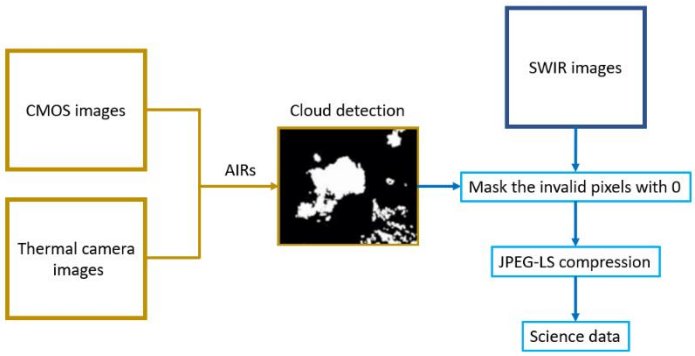

Figure 22. Data handling flowchart in AIRs

2.5.6 Electronic Power System (EPS)

2.5.6.1 Structure

The goal of the Electronic Power System is to provide electricity so that each subsystem and the payload can have sufficient electrical power to carry out the mission. The EPS of GOMI SAT is comprised of multiple units, being the Power Distribution Unit (iPDU), Battery, Battery Unit, and Power Conditioner Unit (iPCU), respectively. The structure of the entire EPS is as follows (Figure 23Schematic of EPS):

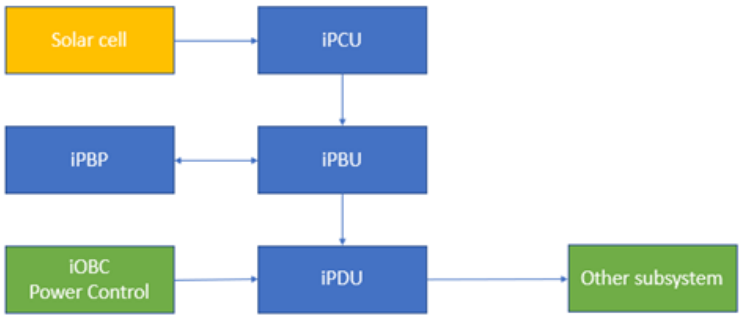

Figure 23. Schematic of EPS

The EPS of GOMI SAT implements Modular Electric Power System of ISIS Space. Since GOMI SAT has two extended solar panels, an iPCU is used to regulate the electricity input to EPS. The iPBU will receive electricity from iPCU and provides electrical power to iPBP and iPDU. The Power Control Unit (PCU) in C&DH will control iPDU to apply power to subsystems.

Table 38 Power Budget in Each Mode

Mode / Bus		Phoenix	Stand-by	Payload	Communication	Propulsion	Detumbling	Safe
TCS		0	0	18	0	0	0	0
ADCS	XACT-50	0	1	6	6	6	6	1
	GPS	0	2	2	2	2	0	0
RCS	MEPSI	0	0	0	0	~0	0	0
EPS	iPCU	0	0	0.397	0	0.397	0.397	0.397

	iPBU	0	0.063	0.063	0.063	0.063	0.063	0.063
	iPDU	0	0.066	0.066	0.066	0.066	0.066	0.066
OBC	iOBC	1	1	1	1	1	1	1
COM	TXS	0	0	0	13	0	0	1.3
	S-Antenna	0	0	0	2	0	0	0.1
	U/VHF Reciever	0	0	0	1	0	0	0.1
	U/VHF antenna	0	0	0	0.15	0	0	0.3
Payload	CCD1	0	0	6	0	0	0	0
	CCD2	0	0	6	0	0	0	0
	CMOS	0	0	0.845	0	0	0	0
	Microbolometer	0	0	0.5	0	0	0	0
	GNSS Reflectometer	0	0	3	0	0	0	0
Sum		1	4.129	43.871	25.279	9.526	7.526	4.326
Margin		0.1	0.4129	4.3871	2.5279	0.9526	0.7526	0.4326
Total (Wh)		1.1	4.5419	48.2581	27.8069	10.4786	8.2786	4.7586

2.5.6.2 Solar Panel

GOMI SAT has two extended solar panels, where are 80 solar cells in total. There are many factors that influence the conversion efficiency of solar panels, including the solar radiation received, the incident angle of the light, the efficiency of individual solar cells, the total surface area, and the number of solar cells. Considering the factors above, the following equations are applied.

$$P_{generation} = n \times A \times \eta_{sc} \times \phi_{sun} \times \cos\beta \times e \tag{2.5.15}$$

Table 39 Parameter of solar panel

n	Number of solar cells $(=80)$
A	Area per solar cell $(=0.0027m^2)$
η_{sc}	Solar cell efficiency $(=0.3)$
ϕ_{sun}	Solar constant $(=1367W/m^2)$
β	Angle of incidence of sun
e	Constants in Umbra and Penumbra $(=0,0.5,1)$

2.5.6.3 Batteries

Since GOMI SAT is a passive telemetry satellite, payload mode will not be activated when the satellite is in Umbra and Penumbra. Hence, communication mode is the most power-consuming mode. To satisfy this condition, GOMI SAT utilizes a 45Wh battery unit that holds more energy than consumption. Another 45Wh battery is used for backup to insure emergency.

2.5.6.4 Analysis

To determine whether GOMI SAT has enough electrical power to support, the equation below

is applied,

$$E_{battery} = E_{generation} - E_{consumption} \tag{2.5.16}$$

After the analysis, the following diagram confirms that **EPS satisfies the requirement of GOMI SAT.**

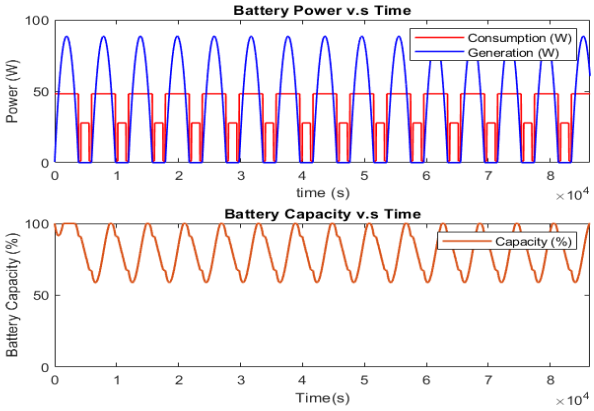

Figure 24. EPS satisfies the requirement of GOMI SAT

3. Originality and social effects

Over the past decades, many inventions meant to help turns out to be harmful nowadays. One of them is plastic. It is known that plastic takes a long time to decompose, which already causes serious environmental problems. But it is not just the environment that is getting affected. In the ocean, persistent organic pollutants, such as DDTs and PCBs, tend to attach on the surface of small pieces of plastic, known as microplastic (smaller than 5mm). If plastic debris is then consumed by marine creatures, pollutants will accumulate in their bodies. Unfortunately, humans will eventually be the final resting place of these pollutants since we are at the top of the food chain. In fact, plastic is threatening our health in a very subtle but severe way!

In the past few years, more and more people are getting aware of this issue and scientists have tried to monitor the movement pattern of plastic litter in the ocean. Sampling directly on the ocean surface with research ships is the most direct method. However, the data acquired by towing techniques lacks real spatial distribution and variation over time. Furthermore, the efficiency is extremely low, and it is almost impossible to sample the entire ocean. Thus, scientists turned their attention to remote sensing. At first, they tried to use existing satellites to detect plastic litter. However, the detection effect is not good because of the payload of these satellites is not designed for plastic litter. With the increasing pollution of the ocean, people urgently need a monitoring system that can monitor marine plastic litter in real time. Luckily, GOMI SAT is here to help!

The payload according to the optical characteristics of plastic litter was designed and applied on GOMI SAT. As a satellite, GOMI SAT can monitor much larger areas periodically and efficiently. It will be the best supplement, if not a great leap forward, to current research on plastic marine litter!

4. Development, manufacture, and launch schedule and manufacturing budget

GOMI SAT will be developed by the NCKU team, associated with several institutes including Physics, Plasma and Space Science, Space Science, Aeronautics & Astronautics, Electrical Engineering Department in NCKU. The cost budget for GOMI SAT is listed below.

Table 40 Cost Budget

Cost Budget for GOMI SAT constellation (Euro)					
SMS		ADCS		Payload	
6U structure	7350	XACT-50	155000	SWIR 1 Camera	3443
Side panels*4	450	MEPSI	100000	SWIR 2 Camera	3443
EPS		TCS		CMOS Camera	14700
iPCU	4400		10000	Thermal Camera	3137
iPBU	3300	TT&C		GNSS-R	1800
iPBP	12800	TXS	8500	GNSS-R antenna	10000
iPDU	4400	S-Antenna	2150	OBC	
Solar panel	55600	U/VHF Reciever	6000	iOBC	4400
Solar cell		U/VHF antenna	11000	Number of CubeSat	6
Launch price	1000000				
Total Cost (Euro)					
3531238					

According to the Development Process Overview of NASA's CubeSat Launch Initiative (CSLI), a mission phase timeline can be plotted below. GOMI SAT Mission, from concept development, design, building, testing and launch, the whole process takes about two and a half years.

Figure 25. Development, manufacture, and launch schedule

5. Conclusion

With the increase in marine pollution, the impact of marine pollution has become increasingly serious. Among them, microplastics pose a great threat to humans and ecology due to biological accumulation. Scientists are anxious to simulate and detect the movement patterns of microplastics, but they are stuck in the lack of complete and rapidly updated sampling data. The GOMI SAT mission provides a solution to this challenge. At LEO, The GOMI SAT equipped with sensors designed for the measurement of the physical properties of microplastics to monitor the global distribution of microplastics. Furthermore, the GOMI SAT mission monitors the temperatures of ocean surface, ocean currents and wind speeds which would are useful information for the improvement of theoretical model. The GOMI SAT mission has the potential to change the way

human study microplastics and play an important role on the UN Sustainable Development Goals (SDG).

6.Reference

[1] Maximenko, N., Corradi, P., Law, K. L., Van Sebille, E., Garaba, S. P., Lampitt, R. S.& Thompson, R. C. (2019). Towards the integrated marine debris observing system.

[2] RESMALI, European Space Agency contract report. Remote Sensing for Marine Litter. 13. Dec 2019.

[3] Garbage Patch Visualization Experiment. https://svs.gsfc.nasa.gov/4174.

[4] "6U CubeSat Design Specification Rev. PROVISIONAL," The CubeSat Program, Cal Poly SLO, URL: https://static1.squarespace.com/static/5418c831e4b0fa4ecac1bacd/t/573fa2fee321400346075f01/1463788288448/6U_CDS_2016-05-19_Provisional.pdf [cited 5 Jul 2020].

[5] Asada, S., Abe, N., Andoh, K., and Fleeter, R. "Launching Small Satellites on the H-IIA Rocket," 17th Annual AIAA/USU Conference on Small Satellites. Utah State University, 2003.

[6] Blue Canyon Technologies. Retrieved from https://storage.googleapis.com/blue-canyon-tech-news/1/2020/06/BCT_DataSheet_Components_ACS_06_2020.pdf

[7] S. R. Strain and J. Eterno. (2011). *NASA Attitude Determination and Control System Techincal Report.* Retrieved from NASA Goddard Space Flight Center.

[8] S.H. Wu. (2011). *Design and Implementation of a Picosat Attitude Control Subsystem.* National Cheng Kung University, Tainan, Taiwan.

[9] M. Navabi, M. R. Hosseini. (2017). Spacecraft Quaternion Based Attitude Input-Output Feedback Linearization Control Using Reaction Wheels. *IEEE.* Doi: 10.1109/RAST.2017.8002994

[10] R. Achanta, A. Shaji, K. Smith, A. Lucchi, P. Fua, S. Süsstrunk. (2012). SLIC Superpixels Compared to State-of-the-Art Superpixel Methods. *IEEE Transactions on Pattern Analysis and Machine Intelligence.* Advance online publication. Doi: 10.1109/TPAMI.2012.120

[11] M. Shi, F. Xie, Y. Zi, J. Yin. (July, 2016). CLOUD DETECTION OF REMOTE SENSING IMAGES BY DEEP LEARNING. *IEEE International Geoscience and Remote Sensing Symposium (IGARSS).* Symposium conducted at Beijing, China.